Journal of Science and Transport Technology
Journal homepage: https://jstt.vn/index.php/en

Design and Inverse Kinematics of Continuum Robots

Duong Van Lac[1], Chau Vu Long[1], Nguyen Manh Hung[1], Vu Quang Van[1], Bui Tien Son[2]

[1]Department of Mechatronics, School of Mechanical Engineering, Hanoi University of Science and Technology (HUST)

[2]Department of Science and Technology, Hanoi University of Industry (HaUI)

Article info
Type of article:
Original research paper

DOI:
https://doi.org/10.58845/jstt.utt.2026.en.6.1.101-111

***Corresponding author:**
Email address:
lac.duongvan@hust.edu.vn

Received: 07/04/2025
Received in Revised Form: 01/12/2025
Accepted: 22/02/2026

Abstract: Continuum robots, characterized by their hyper-redundant and flexible structures, have gained significant attention in fields such as minimally invasive surgery, remote inspection, and soft manipulation. Their complex design and highly nonlinear kinematic behavior present substantial modeling and control challenges. This paper presents a complete framework encompassing the design, modeling, and inverse kinematics solution for a novel two-segment, tendon-driven continuum robot utilizing an elastic spring backbone for enhanced compliance and structural simplicity. A constant curvature forward kinematic model is presented. Subsequently, an efficient numerical approach for solving the challenging inverse kinematics problem is introduced by adapting the Jacobian-based Newton-Raphson method and incorporating the Moore-Penrose Pseudoinverse. This strategy effectively manages the robot's redundancy, ensuring smooth and reliable trajectory generation. Experimental verification confirms the robot's feasibility, demonstrating that the system successfully navigates along the trajectories computed by the inverse kinematics, thus validating the reasonableness of the kinematic model and ensuring seamless and smooth operation. These findings provide a robust foundation for improving motion planning of simple continuum robot platforms in practical applications.

Keywords: Tendon-driven systems, continuum robots, robot kinematics.

1. Introduction

Continuum robots, often referred to as hyper-redundant manipulators, represent a paradigm shift from traditional discrete-jointed robotic systems, drawing inspiration from biological structures such as the elephant trunk, octopus limbs, and snake locomotion [1], [2], [3]. These systems are characterized by their continuous backbone, theoretically possessing infinite degrees of freedom (DOFs), which grants them exceptional flexibility and high dexterity, allowing them to navigate through highly cluttered or confined environments [4], [5]. This unique capability has positioned continuum robots as indispensable tools across several demanding applications. In medicine, they are crucial for minimally invasive surgery (MIS) [6], [7], [8], [9] and specific tasks where small diameters and inherent compliance are critical [10]. Beyond the clinical context, their ability to traverse complex spaces has proven valuable in urban search and rescue following disasters [11], while other designs, like the vine robots [12], offer novel approaches to exploration and environmental interaction. The

core challenge in utilizing these highly adaptable systems lies in accurately modeling their complex shape changes and developing robust solutions for control.

The mechanical realization of continuum robots has evolved considerably since early conceptual designs [13], [14], primarily categorized by their actuation mechanism. Tendon-driven (cable-driven) robots are a foundational design, where actuation cables routed through the robot's body control its bending via differential tension, a concept extensively explored in early continuum robot implementations [2], [13]. Subsequent research has led to more specialized structures to meet application demands. concentric tube robots (CTRs) utilize nested, pre-curved elastic tubes that rotate and translate relative to one another to control the overall shape [15], and their mechanics and calibration are particularly complex [16]. Another significant avenue involves incorporating extensible sections within the robot's body, which adds axial movement to the bending capability, complicating the modeling but increasing dexterity and access range [2], [17]. Regardless of the actuation method (tendon, pneumatic, or telescoping tubes), a critical area of investigation remains the comprehensive modeling of statics and dynamics, especially considering the influence of friction, external loads, and gravitational effects on the continuous body structure [5], [18].

The kinematic modeling of continuum robots is essential for predicting the end-effector pose based on actuator inputs. Due to the hyper-redundancy and inherent flexibility, this process requires careful simplification. The constant curvature (CC) model is the most prevalent approach, simplifying the robot's curvature into a series of circular arcs for each segment [7], [10], [19]. This model offers simple analytical solutions, making it highly suitable for real-time control. However, for applications requiring higher accuracy or when significant external forces are present, more rigorous methods are necessary. The piecewise constant curvature (PCC) approximation extends the CC model by dividing the continuum backbone into smaller segments [20]. Beyond these approximations, researchers have successfully applied Modal Kinematics, first proposed by Chirikjian and Burdick, which uses a finite set of shape functions (or modes) to represent the robot's configuration [17], [12], [21]. For true physical fidelity, the Cosserat Rod Theory provides a continuum mechanics-based approach that rigorously accounts for bending, torsion, and shear, essential for analyzing the elastic stability and behavior of robots under loading [8], [22], [23], [24], particularly for multi-backbone systems.

Solving the inverse kinematics problem, determining the necessary actuator commands to achieve a desired end-effector position and orientation, is notoriously difficult for hyper-redundant systems [25], [26]. Due to the nonlinear relationship between actuator space and task space, the most widely adopted solutions are numerical and iterative. Jacobian-based methods are the standard, utilizing the robot's geometric Jacobian to compute the instantaneous relationship between joint and end-effector velocities [27]. While Jacobian methods are robust, non-analytical solutions, such as the FABRIKx algorithm, are also being explored to tackle the complexity of variable curvature robots [28]. Finally, the realization of accurate, repeatable motion necessitates transitioning from open-loop control to closed-loop control [20]. This requires robust kinematic calibration and effective sensor integration to address modeling errors and unmodeled effects, such as friction, coupling, and backlash, which are significant in tendon-driven systems [24], [29], [30], [31], [32]. Furthermore, sensing capabilities, including the use of intrinsic force sensing, is critical for real-world interaction and control [11].

Building upon established literature, this paper presents a comprehensive framework for the design, modeling, and control of a two-segment continuum robot. The primary contributions include the mechanical design, which utilizes an elastic

spring backbone for inherent compliance and simplified assembly, and an efficient kinematic modeling approach. The robot design is open-source and available at: https://github.com/lacduong/ContinuumRobot. Crucially, the inverse kinematics solution employs the Newton-Raphson method combined with the Moore-Penrose pseudoinverse to handle redundancy, ensure high reliability, and generate smooth trajectories. The efficacy of this framework is validated experimentally, demonstrating strong consistency between the calculated trajectories and the robot's actual motion.

The remainder of the paper is organized as follows: Section 2 details the mechanical design; Section 3 develops the kinematic model; Section 4 presents the inverse kinematics solution; Section 5 provides experimental validation and discusses the limitations; and Section 6 concludes the paper and outlines future work.

2. Design

Configuration selection is a critical aspect of robot design. A three-tendon configuration was chosen over a four-tendon design due to its cost efficiency, simplified control, and reduced weight. The robot's backbone is constructed using elastic springs, selected for their availability, ease of fabrication, and ability to meet the required elasticity specifications.

Each segment bends smoothly under controlled cable tension, with flexible joints maintaining continuous curvature. The tendons are routed through holes in dividing plates and anchored at the base, where servo motors regulate their tension. To ensure efficient force transmission and precise bending control, lubricants are applied at each hole to minimize friction. The design prioritizes simplicity and dexterity, making it ideal for tasks requiring high flexibility without axial elongation or torsion resistance. The robot consists of two 155 mm segments, each divided into five flexible sections. Each segment is actuated by three tension cables symmetrically arranged around a central axis. These cables pass through holes positioned 22 mm from the center of 50 mm diameter circular plates, which guide the cables and separate the segments. Fig. 1 illustrates the complete design, including the segmented plate structure, with its parameters listed in Table 1. Each segment is controlled by three servo motors, with each motor adjusting the length of a single cable to achieve the desired bending motion.

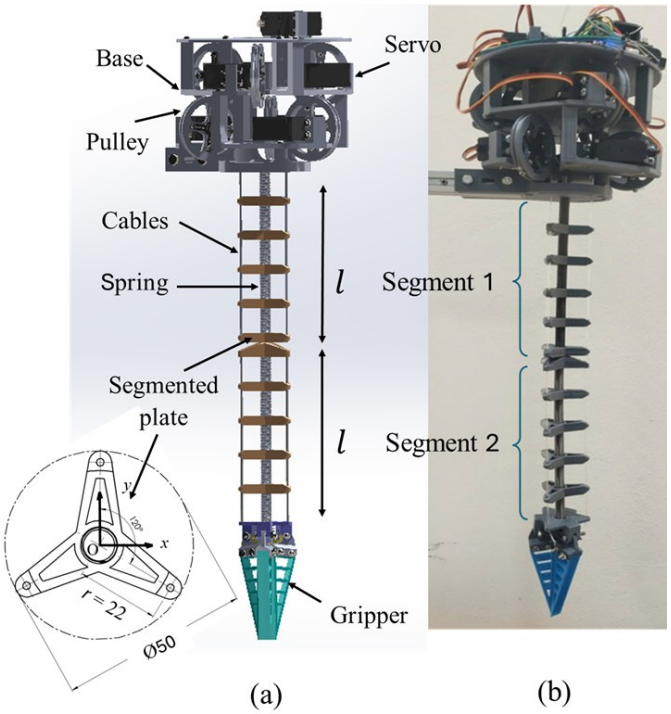

Fig. 1. (a) 3D design model (b) Real robot

Table 1. Robot Parameters

Parameter	Value	Units
Total mass	527.04	g
Mass of each segment	37.6	g
Pulley mass	7.2	g
Length of each segment	155	mm
Spring wire diameter	0.8	mm
Bending limit angle	[0, 90]	°
Rotation angle limit	[0, 360]	°

3. Kinematics Modeling

Modeling tendon-driven robots (TDRs) is an important and rapidly growing area of research [6], [13], [17], [32]. Unlike rigid robots (RRs), which primarily rely on joint variables to define their configuration, the behavior of soft robots (SRs) including TDRs is significantly influenced by the elasticity of their materials. Early modeling approaches were often complex and required strong simplifying assumptions to remain analytically tractable. One widely adopted method is the constant curvature assumption, which simplifies kinematic analysis by representing the robot's shape as a circular arc, defined using arc parameters. In our approach, as illustrated in Fig. 2, we first present the transformation from an intermediate parameter space defined by k, ϕ, and l (or more compactly, θ and ϕ, due to the interdependence among k, l, and θ, with the relation $k=\frac{1}{r}$, leading to $\theta = \frac{l}{r} = lk$) to the workspace. Next, we rigorously derive the relationship between the arc parameters θ and ϕ, and the tendon lengths. This mapping forms the foundation for controlling the end-effector position via tendon actuation. Descriptions of the remaining symbols can be found in Table 2.

In this study, the constant curvature assumption is employed to develop a simplified kinematic model, focusing on angular parameters for subsequent calculations. This approach not only reduces computational complexity but also benefits from the mathematical convenience introduced by the assumption. The homogeneous transformation matrix of a segment is defined as:

$$T=\begin{bmatrix} R_z(\phi) & 0 \\ 0 & 1 \end{bmatrix}\begin{bmatrix} R_y(\theta) & p \\ 0 & 1 \end{bmatrix} \quad (1)$$

The result of the transformation (1) is

Table 2. Notation and Definition

Symbol	Units	Definition
k	mm^{-1}	Robot curvature
ϕ	rad	Robot twist angle around z-axis
θ	rad	Robot bending angle around y-axis
r	mm	Robot curvature radius
l	mm	The initial length of each tendon
x_i, y_i, z_i	mm	The coordinates of the end point of the segment *i*

$$T=\begin{bmatrix} \cos\phi\cos\theta & -\sin\phi & \cos\phi\sin\theta & r\cos\phi(1-\cos\theta) \\ \sin\phi\cos\theta & \cos\phi & \sin\phi\sin\theta & r\sin\phi(1-\cos\theta) \\ -\sin\theta & 0 & \cos\theta & r\sin\theta \\ 0 & 0 & 0 & 1 \end{bmatrix} \quad (2)$$

Thus, homogeneous transformation matrices are employed to calculate the endpoint coordinates of a segment, as follows

$$\begin{bmatrix} x_E \\ y_E \\ z_E \end{bmatrix} = \begin{bmatrix} r\cos\phi\,(1-\cos\theta) \\ r\sin\phi\,(1-\cos\theta) \\ r\sin\theta \end{bmatrix} \quad (3)$$

The forward kinematics equation (3) results in

$$\begin{cases} \phi = \tan^{-1}\dfrac{y_E}{x_E} \\ \beta = \tan^{-1}\dfrac{\sqrt{{y_E}^2+{x_E}^2}}{z_E} \\ \theta = \begin{cases} 2\beta\ (\text{if } z_E > 0) \\ \pi\ (\text{if } z_E = 0) \\ 2\pi + 2\beta\ (\text{if } z_E < 0) \end{cases} \end{cases} \quad (4)$$

Fig. 3 illustrates the transformation from the intermediate space to the tendon length. Based on this representation, the relationship can be derived as follows:

$$r_i = r - d\cos\alpha_i \quad (5)$$

where α_i is the angle formed between tendon *i* and a straight line connecting the center of the base to the center of the top plate, as shown in Fig. 3. The subscript *i* denotes the index of the tendon. Multiplying both sides of (5) by the angle θ, we obtain:

$$l_i = l - d\theta\cos\alpha_i \quad (6)$$

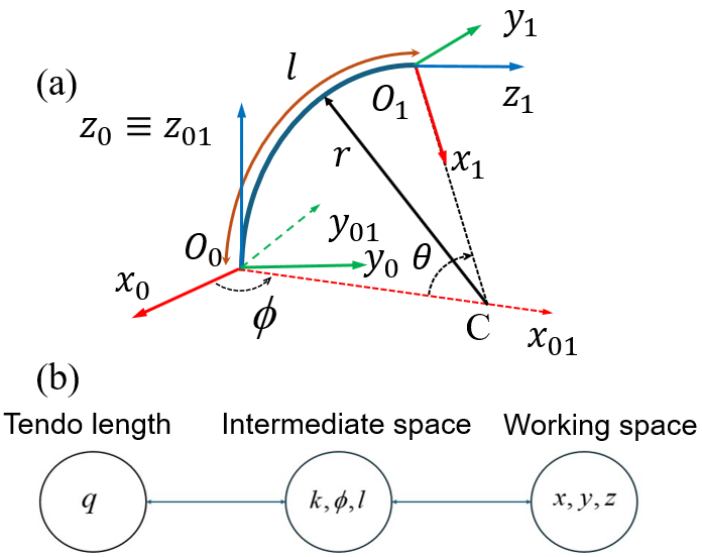

Fig 2. (a) Geometric representation of a continuum robot segment, showing its arc and bending configuration. (b) Diagram depicting the mapping from actuation space to intermediate space, and subsequently to working space

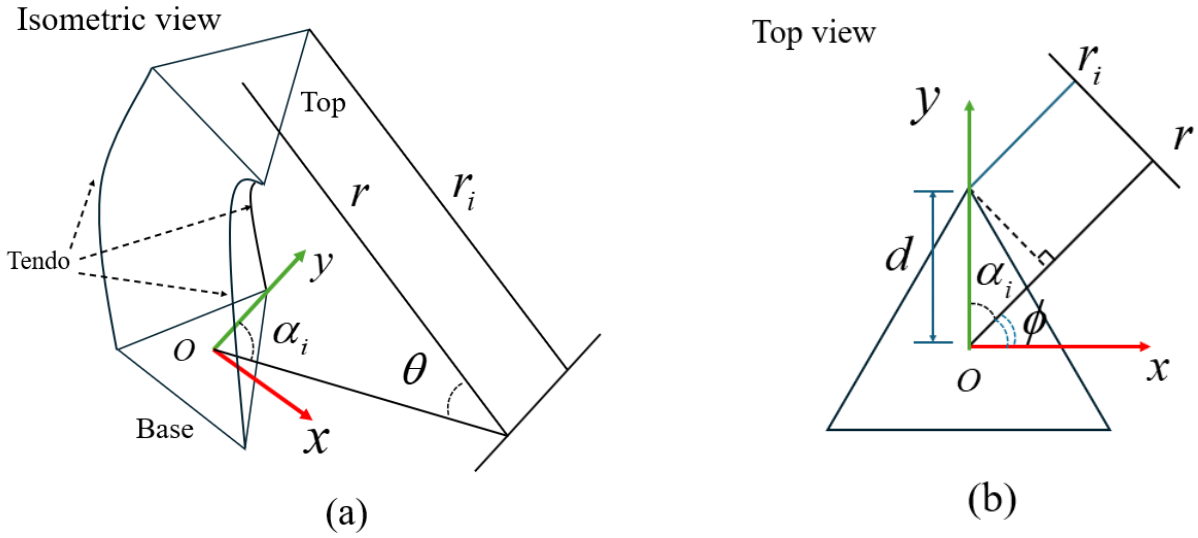

Fig. 3. Representation of parameters in the transformation from intermediate space to tendon length. (a) Isometric view of a bent segment. (b) Top view.

Due to the design, the angles are offset by $\pi/3$, so the corresponding angles α_i are:

$$\begin{cases} \alpha_1 = \dfrac{\pi}{2} - \phi \\ \alpha_2 = \dfrac{7\pi}{6} - \phi \\ \alpha_3 = \dfrac{11\pi}{6} - \phi \end{cases} \quad (7)$$

Substituting the values from (7) into (6), we obtain the tendon length l_i. As shown in Fig. 4, the variation in tendon lengths is determined by adjusting the servo rotation angles according to

$$l - l_i = R\gamma_i \quad (8)$$

where R denotes the radius of the flywheel, and γ_i represents to the rotation angle of the servo motor; l is the initial cable length, while l_i is the cable length after the motor has rotated by an angle γ_i.

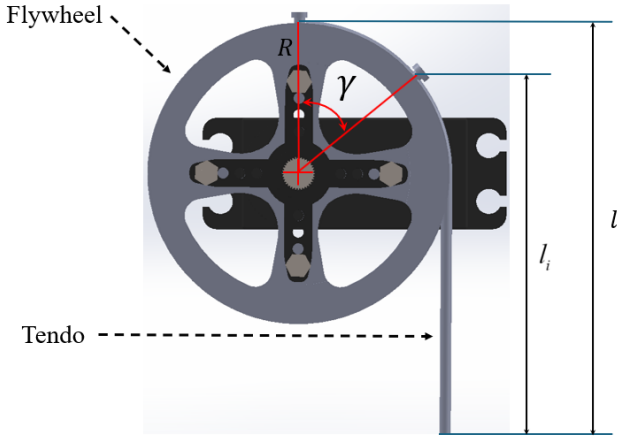

Fig. 4. The actuation mechanism of a tendon

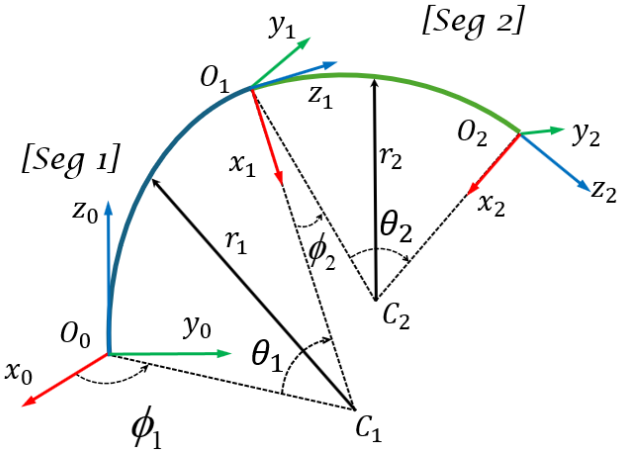

Fig. 5. Two-segment continuum robot configuration

The coordinates of the endpoint of the first segment is

$$\begin{bmatrix} x_1 \\ y_1 \\ z_1 \end{bmatrix} = \begin{bmatrix} r\cos\phi_1\,(1-\cos\theta_1) \\ r\sin\phi_1\,(1-\cos\theta_1) \\ r\sin\theta_1 \end{bmatrix} \quad (9)$$

The coordinates of the endpoint of the second segment are determined as ${}^0T_2 = {}^0T_1{}^1T_2$. Substituting the angular variable values as shown in Fig. 5, and after simplification, the final impact point coordinates are obtained: (10)

$$\begin{bmatrix} x_2 \\ y_2 \\ z_2 \end{bmatrix} = \begin{bmatrix} x_1 + r_2\cos\phi_1\sin\theta_1\sin\theta_2 + r_2\sin\phi_1\sin\phi_2(\cos\theta_2 - 1) \\ - r_2\cos\phi_1\cos\phi_2\cos\theta_1(\cos\theta_2 - 1) \\ y_1 + r_2\sin\phi_1\sin\theta_1\sin\theta_2 - r_2\cos\phi_1\sin\phi_2(\cos\theta_2 - 1) \\ - r_2\cos\phi_2\cos\theta_1\sin\phi_1(\cos\theta_2 - 1) \\ z_1 + r_2\cos\theta_1\sin\theta_2 + r_2\cos\phi_2\sin\theta_1(\cos\theta_2 - 1) \end{bmatrix}$$

4. Inverse Kinematics

Solving the kinematics problem of robotic manipulators, especially those with compliant or redundant structures like continuum robots, typically involves addressing a set of highly nonlinear equations. The inherent redundancy in continuum robots, where the number of configuration angles ($\mathbf{X} = [\phi_1 \quad \theta_1 \quad \phi_2 \quad \theta_2]^T$) exceeds the number of required task-space variables ($\mathbf{p}_E^d = [x_2, y_2, z_2]^T$) means that a unique solution does not exist. To manage this challenge and find a practical, accurate solution, this study customized the traditional Newton-Raphson method and incorporated the Moore-Penrose inverse. This hybrid approach provides accurate approximations and reliable simulation results for determining the robot's configuration.

Given the desired end-effector pose $\mathbf{p}_E^d$, the inverse kinematics problem, which relates the task space to the joint space, derived from equation (10), can be fundamentally formulated as:

$$\mathbf{p}_E^d = \mathbf{f}(\mathbf{X}) = \begin{bmatrix} f_1(\mathbf{X}) \\ f_2(\mathbf{X}) \\ f_3(\mathbf{X}) \end{bmatrix} \quad (11)$$

The primary mathematical challenge in solving (11) is the aforementioned redundancy, where the system is underdetermined. The core idea behind using the iterative Newton-Raphson

method is to linearize the function $\mathbf{f}(\mathbf{X})$ around a current estimate $\mathbf{X}_\mathrm{k}$ and iteratively refine the solution to minimize the error between the desired pose and the current forward kinematics solution. The proposed computational formula, which incorporates the Jacobian's pseudoinverse to handle the redundancy, can be expressed in an iterative form as:

$$\mathbf{X}_{\mathrm{k+1}} = \mathbf{X}_\mathrm{k} + \mathbf{J}^{\dagger}(\mathbf{X}_\mathrm{k})(\mathbf{p}_\mathrm{E}^\mathrm{d} - \mathbf{f}(\mathbf{X}_\mathrm{k})) \quad (12)$$

Here, $\mathbf{J}^{\dagger}$ is the Moore-Penrose inverse (or pseudoinverse) of the Jacobian matrix $\mathbf{J}$. The pseudoinverse plays a crucial role as it provides the minimum norm solution in the sense of least squares, effectively selecting the joint-space velocity solution ($\Delta\mathbf{X}$) that has the smallest magnitude, which is physically desirable for stable robot motion. The Jacobian of the forward kinematics function is formally defined as:

$$\boldsymbol{J} = \frac{\partial \boldsymbol{f}}{\partial \boldsymbol{X}} = \begin{bmatrix} \frac{\partial f_1}{\partial \phi_1} & \frac{\partial f_1}{\partial \theta_1} & \frac{\partial f_1}{\partial \phi_2} & \frac{\partial f_1}{\partial \theta_2} \\ \frac{\partial f_2}{\partial \phi_1} & \frac{\partial f_2}{\partial \theta_1} & \frac{\partial f_2}{\partial \phi_2} & \frac{\partial f_2}{\partial \theta_2} \\ \frac{\partial f_3}{\partial \phi_1} & \frac{\partial f_3}{\partial \theta_1} & \frac{\partial f_3}{\partial \phi_2} & \frac{\partial f_3}{\partial \theta_2} \end{bmatrix} \quad (13)$$

The complete inverse kinematics algorithm is implemented using the iterative process defined by equation (12) as follows:

Input: The desired end-effector pose $\boldsymbol{p}_E^\mathrm{d}$

Output: Configuration angles $\boldsymbol{X}$

Step 1: Initialize the iteration: Set the iteration counter $\mathrm{k} = 0$, choose an initial guess $\mathbf{X}_0$, define the maximum number of iterations N, and set the convergence tolerance ϵ.

Step 2: Execute the iterative loop for k = 0, 1, …, N-1:

(a) Compute the Moore-Penrose inverse $\boldsymbol{J}^{\dagger}(\boldsymbol{X}_k)$and the current end-effector pose $\boldsymbol{f}(\boldsymbol{X}_k)$ at the current configuration $\boldsymbol{X}_k$.

(b) Update the configuration angles using the difference between the desired and current pose, scaled by the pseudoinverse (12).

(c) Check convergence by evaluating the error magnitude: If $\left\|\boldsymbol{p}_E^d - \boldsymbol{f}(\boldsymbol{X}_{k+1})\right\| < \epsilon$, the solution has converged, and the process is terminated.

The choice of the initial condition $\boldsymbol{X}_0$ is vital for ensuring both rapid convergence and the physical plausibility of the resulting robot configuration. When the robot is following a trajectory, a series of desired endpoints $\boldsymbol{p}_E^d(t_n)$ over time, it is critical to maintain smooth movement. This is achieved by using the solution from the previous time step as the initial guess for the current step: $\boldsymbol{X}_0(t_{n+1}) = \boldsymbol{X}(t_n)$. This methodology ensures that the robot's configuration at time t_{n+1} is minimally perturbed from its configuration at t_n. Consequently, the iterative calculation converges quickly in a few iterations, and the physical robot executes smooth, continuous motion.

For this study, the convergence tolerance ϵ was set to a high precision of 10^{-6}, though this value is adjustable based on the required application accuracy. The maximum number of iterations N was conservatively chosen as 100. To validate the proposed inverse kinematics method, the robot's resulting shape was examined for a specific target point in the workspace. The desired endpoint was set at the spatial coordinate $\boldsymbol{p}_E^d = (100, -100, 230)^T$ mm, as visually depicted in the simulation results in Fig. 6.

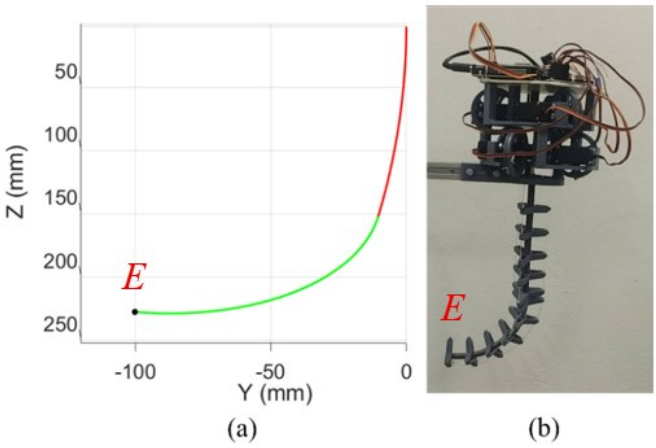

Fig. 6. (a) Simulated shape of the robot, (b) actual performance on the real robot

The converged solution for the configuration angles vector yielded the values: ϕ_1 = 5.8336, θ_1 =

0.3105, ϕ_2 = 5.7595, θ_2= 1.4306. These joint angles subsequently translated into the following motor angles necessary for physical actuation: γ_1 = 83°, γ_2 = 81°, γ_3 = 105°, γ_4 = 32°, γ_5 = 85°, and γ_6 = 154°. The successful and precise convergence to this target point validates the robustness and accuracy of the inverse kinematics approach based on the customized Newton-Raphson method with the Moore-Penrose inverse.

5. Simulations and Experiments

This section serves to verify the computational capability of the proposed inverse kinematics algorithm against complex trajectories and to validate the model's reliability through comparison with the robot's actual physical operation. To test the algorithm's reliability in motion planning, the robot's movement was simulated along two fundamental paths. Fig. 7(a) and (b) illustrate the robot's motion along straight and circular paths, respectively, demonstrating that the robot's configuration transitions seamlessly at every point. This outcome successfully indicates the algorithm's ability to calculate the required sequence of joint configurations, allowing the robot to follow predefined trajectories smoothly and accurately.

Furthermore, to validate the model's correspondence with reality, Fig. 8 presents the correlation results between the simulation and the real robot's performance as it traverses a straight line from point A(201, 139, 104) mm to point B(228, -68, 104) mm across the time interval t = 0, 0.2, … 1 (s). The visual and quantitative comparison confirms that the robot's configuration, both in calculation and experimental testing, is highly similar, thereby confirming the reliability and fidelity of the proposed inverse kinematics method for continuum robots.

However, it is crucial to note the current limitations in control. The primary scope of this research has been strictly focused on the design of the continuum robot and the resolution of the Inverse Kinematics problem. Consequently, the current assessment of the robot's ability to execute calculated configurations is primarily qualitative. The robot operates in an open-loop manner, relying entirely on the pre-calculated joint commands derived from the kinematic model. This setup currently lacks external feedback sensors, meaning it cannot automatically compensate for positional errors arising from complex physical effects such as cable slack, material compliance, friction, or external loading. The accuracy of the motion is thus solely dependent on the accuracy of the underlying kinematic model.

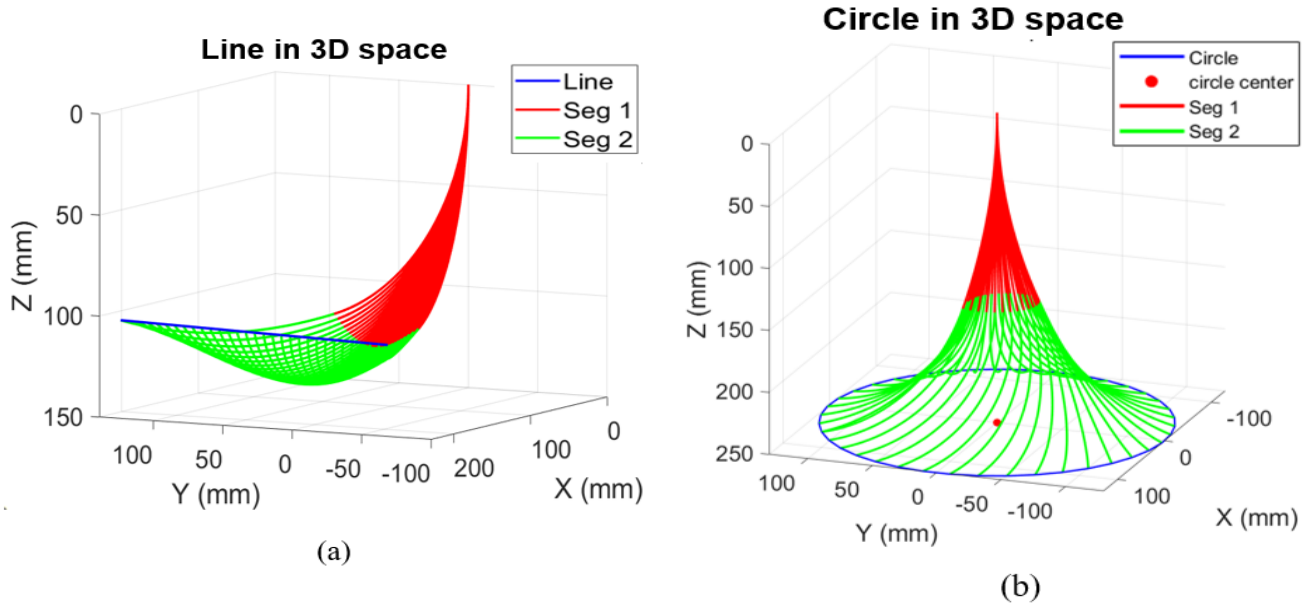

Fig. 7. Simulated results, (a) Straight-line trajectory, (b) Circular trajectory

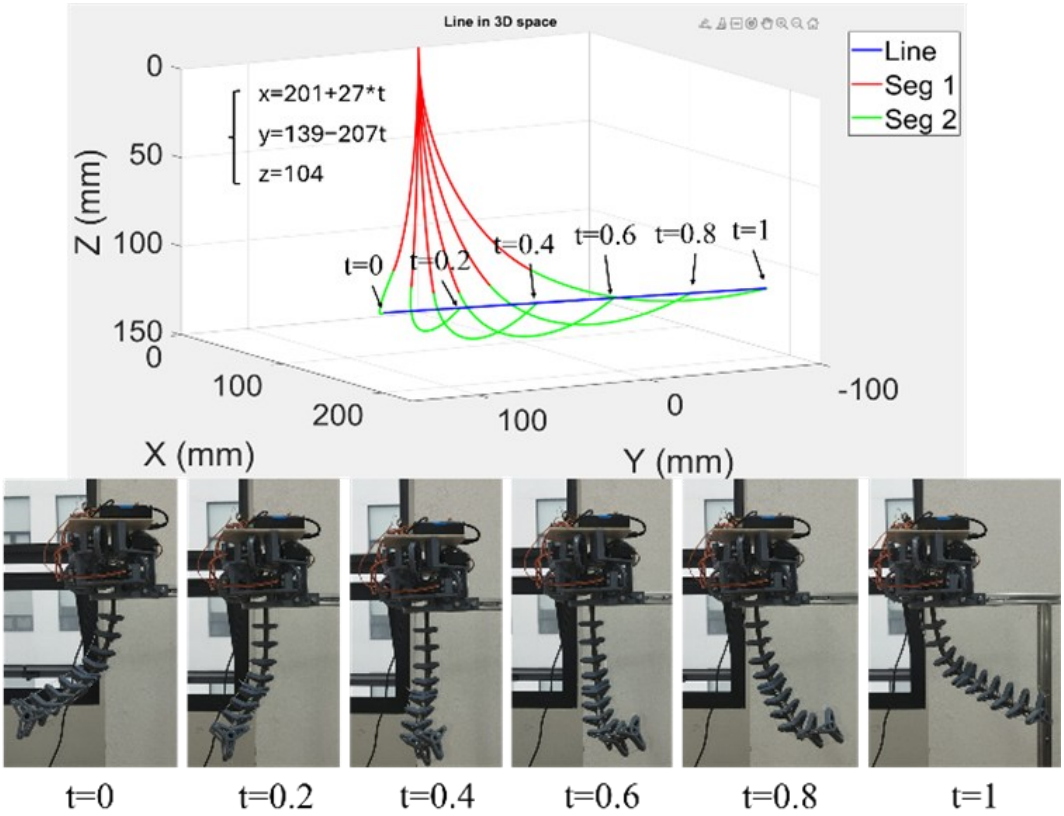

Fig. 8. Comparing the motion of the simulated and real robot while moving along the straight-line trajectory

To fully transition this work from a successful kinematic analysis to a practical, high-precision robotic system, future research must address closed-loop control. This will involve integrating sensing technologies such as Fiber Bragg Grating (FBG) sensors along the backbone to enable real-time shape sensing, or utilizing vision-based systems to track the end-effector's actual position. Incorporating these sensors will allow for the development of robust Jacobian-based kinematic control strategies and eventually, the inclusion of dynamic models to handle disturbances. This transition to sensor-integrated control will significantly enhance the robot's precision, adaptability, and ultimate utility in complex application environments.

6. Conclusion

This study successfully presented the design, kinematic modeling, and inverse kinematics solution for a continuum robot. The key technical achievement was the application of the Newton-Raphson method with the Moore-Penrose inverse to solve the inherent redundancy. Simulations and experiments validated the model's efficiency, confirming the robot's ability to follow trajectories smoothly and reliably. However, the current open-loop control necessitates a transition to high-precision closed-loop control. Future work will focus on integrating a feedback system using Fiber Bragg Grating (FBG) sensors and image processing for real-time shape sensing, end-effector localization, and obstacle avoidance. Simultaneously, we will pursue design optimization, including structural configurations, materials, and parameter tuning and investigate modular designs to enhance scalability and overall robot performance.

References

[1] S. Hirose. (1993). Biologically Inspired Robots. *Oxford University Press, U.K.*, pp. 147–155.

[2] M.W. Hannan and I.D. Walker. (2003). Kinematics and the implementation of an elephant’s trunk manipulator and other continuum-style robots. *Journal of Robotic*

Systems, 20(2), 45–63. https://doi.org/10.1002/rob.10070

[3] W. McMahan, B.A. Jones, I.D. Walker, V. Chitrakaran, A. Seshadri, and D. Dawson. (2004). Robotic manipulators inspired by cephalopod limbs. *Proceedings of the CDEN Design Conference, Montreal, QC, Canada, pp. 1–10.*

[4] R. Buckingham. (2002). Snake arm robots. *Industrial Robot*, 29(3), 242–245. https://doi.org/10.1108/01439910210425531

[5] I.D. Walker. (2013). Continuous backbone "continuum" robot manipulators. *International Scholarly Research Notices, ISRN Robotics*, 2013, 726506. https://doi.org/10.5402/2013/726506

[6] J. Burgner-Kahrs, D.C. Rucker, and H. Choset. (2015). Continuum robots for medical applications: A survey. *IEEE Transactions on Robotics*, 31(6), 1261–1280. doi: 10.1109/TRO.2015.2489500

[7] S. Sen, A. Garg, D.V. Gealy, S. McKinley, Y. Jen, and K. Goldberg. (2016). Automating multi-throw multilateral surgical suturing with a mechanical needle guide and sequential convex optimization. *Proceedings of the IEEE International Conference on Robotics and Automation (ICRA), pp. 4178–4185*. doi: 10.1109/ICRA.2016.7487611

[8] J. Till, V. Aloi, and C. Rucker. (2019). Real-time dynamics of soft and continuum robots based on Cosserat rod models. *The International Journal of Robotics Research*, 38(6), 723–746. https://doi.org/10.1177/0278364919842269

[9] N. Simaan, et al. (2009). Design and integration of a telerobotic system for minimally invasive surgery of the throat. *International Journal of Robotics Research*, 28(9), 1134–1153. doi: 10.1177/0278364908104278

[10] T. Veiga, et al. (2020). Challenges of continuum robots in clinical context: A review. *Progress in Biomedical Engineering*, 2, 032003. DOI 10.1088/2516-1091/ab9f41

[11] J. Casper and R.R. Murphy. (2003). Human-robot interactions during the robot-assisted urban search and rescue response at the World Trade Center. *IEEE Transactions on Systems, Man, and Cybernetics*, 33(3), 367–385. doi: 10.1109/TSMCB.2003.811794

[12] M.M. Coad et al. (2020). Vine robots. *IEEE Robotics & Automation Magazine*, 27(3), 120–132. doi: 10.1109/MRA.2019.2947538

[13] G. Immega and K. Antonelli. (1995). The KSI tentacle manipulator. *Proceedings of IEEE International Conference on Robotics and Automation, Vol. 3, Nagoya, Japan, pp. 3149–3154.* doi: 10.1109/ROBOT.1995.525733

[14] K. Suzumori, S. Iikura, H. Tanaka. (1991). Development of flexible microactuator and its application to robotic mechanisms. *Proceedings of IEEE International Conference on Robotics and Automation, Vol. 2, Sacramento, CA, USA, pp. 1622–1627.* doi: 10.1109/ROBOT.1991.131850

[15] R.J. Webster, J.M. Romano, N.J. Cowan. (2009). Mechanics of precurved-tube continuum robots. *IEEE Transactions on Robotics*, 25(1), 67–78. doi: 10.1109/TRO.2008.2006868

[16] C. Jang, J. Ha, P.E. Dupont and F.C. Park. (2016). Toward on-line parameter estimation of concentric tube robots using a mechanics-based kinematic model. *Proceedings of the IEEE/RSJ International Conference on Intelligent Robots and Systems*, pp. 2400–2405. doi: 10.1109/IROS.2016.7759374

[17] E. Amanov, T.-D. Nguyen, J. Burgner-Kahrs. (2021). Tendon-driven continuum robots with extensible sections: A model-based evaluation of path-following motions. *The International Journal of Robotics Research*, 40(1), 7–23. https://doi.org/10.1177/0278364919886047

[18] D.C. Rucker and R.J. Webster III. (2011). Statics and dynamics of continuum robots with general tendon routing and external loading. *IEEE Transactions on Robotics*, 27(6), 1033–1044. doi: 10.1109/TRO.2011.2160469

[19] B.A. Jones and I.D. Walker. (2006). Kinematics for multisection continuum robots. *IEEE Transactions on Robotics*, 22(1), 43–55. doi: 10.1109/TRO.2005.861458

[20] D.B. Camarillo, C.R. Carlson, J.K. Salisbury. (2009). Configuration tracking for continuum manipulators with coupled tendon drive. *IEEE Transactions on Robotics*, 25(4), 798–808. doi: 10.1109/TRO.2009.2022426

[21] G.S. Chirikjian, J.W. Burdick. (1994). A modal approach to hyper-redundant manipulator kinematics. *IEEE Transactions on Robotics and Automation*, 10(3), 343–354. doi: 10.1109/70.294209

[22] K. Xu and N. Simaan. (2010). Analytic formulation for kinematics, statics, and shape restoration of multibackbone continuum robots via elliptic integrals. *ASME Journal of Mechanisms and Robotics*, 2(1), 011006. https://doi.org/10.1115/1.4000519

[23] J. Till and D.C. Rucker. (2017). Elastic stability of Cosserat rods and parallel continuum robots. *IEEE Transactions on Robotics*, 33(3), 718–733. doi: 10.1109/TRO.2017.2664879

[24] L. Wang and N. Simaan. (2014). Investigation of error propagation in multibackbone continuum robots. *Advances in Robot Kinematics, Springer, pp. 385–394*.

[25] S. Neppalli, M.A. Csencsits, B.A. Jones, and I. Walker. (2008). A geometrical approach to inverse kinematics for continuum manipulators. *Proceedings of the IEEE/RSJ International Conference on Intelligent Robots and Systems, Nice, France, pp. 3565–3570.* doi: 10.1109/IROS.2008.4651125

[26] G.S. Chirikjian and J.W. Burdick. (1995). Kinematically optimal hyper-redundant manipulator configurations. *IEEE Transactions on Robotics and Automation*, 11(6), 794–806. doi: 10.1109/70.478427

[27] S.R. Buss. (2004). Introduction to inverse kinematics with Jacobian transpose, pseudoinverse and damped least squares methods. *IEEE Transactions on Robotics and Automation*, 17, 1–19.

[28] D. Kolpashchikov, O. Gerget and V. Danilov. (2022). FABRIKx: Tackling the inverse kinematics problem of continuum robots with variable curvature. *Robotics*, 11(6), 128. https://doi.org/10.3390/robotics11060128

[29] C. Escande et al. (2015). Kinematic calibration of a multisection bionic manipulator. *IEEE/ASME Transactions on Mechatronics*, 20(2), 663–674. doi: 10.1109/TMECH.2014.2313741

[30] B.W. Mooring et al. (1991). Fundamentals of Manipulator Calibration. *Wiley, USA*.

[31] J.M. Hollerbach and C.W. Wampler. (1996). The calibration index and taxonomy for robot kinematic calibration methods. *International Journal of Robotics Research*, 15(6), 573–591. https://doi.org/10.1177/027836499601500604

[32] R. Roy, L. Wang, N. Simaan. (2017). Modeling and estimation of friction, extension, and coupling effects in multisegment continuum robots. *IEEE/ASME Transactions on Mechatronics*, 22(2), 909–920. doi: 10.1109/TMECH.2016.2643640